k-space theory and convective gains of stimulated Raman side scattering

C. Z. Xiao,[1,2,3,*] Q. Wang,[2] and J. F. Myatt[2,†]

[1]*School of Physics and Electronics, Hunan University, Changsha 410082, China*

[2]*Department of Electrical and Computer Engineering, 9211 116 St. NW, University of Alberta, Alberta, Canada T6G 1H9*

[3]*Collaborative Innovation Center of IFSA (CICIFSA), Shanghai Jiao Tong University, Shanghai 200240, China*

(Received 2 November 2022; accepted 19 January 2023; published 6 February 2023)

We have developed a *k*-space theory for stimulated Raman scattering. The theory is used to calculate the convective gain of stimulated Raman side scattering (SRSS) in order to clarify the discrepancies found between previous gain formulas proposed in the literature. The gains are dramatically modified by the eigenvalue of SRSS, and the maximum gain occurs not at the perfect wave-number matching condition but instead at a wave number having a small deviation that is associated with the eigenvalue. Numerical solutions of the *k*-space theory equations are compared with, and used to verify, analytically derived gains. We demonstrate connections to the existing path integral theories, and we derive a similar path integral formula in *k* space.

DOI: 10.1103/PhysRevE.107.025203

I. INTRODUCTION

Stimulated Raman side scattering (SRSS) is a particularly interesting scattering geometry of stimulated Raman scattering (SRS), which has been observed in recent experiments [1–4] and particle-in-cell numerical simulations [5]. As we define it here, it is a scattering geometry where the scattered light grows in a direction that is nearly perpendicular to the local direction of the density gradient. It therefore occurs near the wave caustic/turning point for the scattered light, and the light exits plasma with angles that are modified significantly by refraction. Although the absolute threshold of SRSS [6,7] is rather low, according to theoretical predictions, very few experiments have reported the observation of SRSS previously [8–10]. Recently, the observations of vigorous SRSS in ignition-related experiments have revived the interest of the plasma community in this instability.

There could be several reasons for the lack of previous observations: To capture side scatter, a particular light collecting system is required since the ray trajectory of side scatter light back to detectors is not unique [11] and is strongly affected by refraction. Side scattered light can also be difficult to distinguish from other noise sources scattered or reflected by the plasma. It is only when the SRSS signals are sufficiently strong that it can be unambiguously observed [8]. Other effects such as collisional and Landau damping could also mitigate such scattering easily [12,13]. Its observation would then depend sensitively on the plasma conditions. Furthermore, as we show here, the inherent complexity of SRSS is much greater than for backward scattering. This is a fact that does not seem to have been fully appreciated, and one that we attempt to resolve.

Take, for example, the analytic formulas for convective gains. When the instability is below the absolute threshold, convective gain is used to assess the severity of SRSS. Such a situation can be expected to occur when the pump intensity is not strong enough, the decay waves are strongly damped, the transverse beam size is not sufficiently wide, or the density gradient is too steep. However, there are several different forms of analytically derived gains that have been obtained from different theories [3,14,15]. These formulas appear quite different from one another, and it is not obviously apparent how they should be used under certain conditions in a given experiment. Additionally, they have yet to be verified.

We start by summarizing the previously obtained results for convective SRSS gain. There are two types of theories aimed at calculating the convective gain: *x*-space theory and a path integral method. In the very first theory of convective SRSS, which was made by Mostrom, Nicholson, and Kaufman [15], steady-state solutions of the first-order envelope equations were solved in real space. The formula they obtained for convective gain is equivalent to that recently derived by Michel *et al.* [3] from a standard path integral method, where an integral over the coupling coefficient is performed along the ray trajectory. The reduced analytic formula is given by

$$G = G_{\mathrm{Ros}}(0)\sqrt{\frac{\omega_s^2-\omega_{pr}^2}{\omega_{pr}^2}}\sqrt{\frac{\omega_{pr}}{\nu}}, \tag{1}$$

where $G_{\mathrm{Ros}}(0)$ is the well-known Rosenbluth gain expressed by Eq. (24) (derived below) for backscatter and normal incidence (incidence angle $\theta_0 = 0$), ω_{pr} is the plasma frequency at the resonant point, ω_s is the frequency of scattered light, and ν is the damping rate of the Langmuir wave. Since thermal effects are not included in Eq. (1), Michel *et al.* [3] also found that, in the limit of negligible Langmuir wave damping, the

*xiaocz@hnu.edu.cn

†myatt@ualberta.ca

path integral method reduces to

$$G = G_{\mathrm{Ros}}(0)\frac{k_s c^2}{3v_e^2 k_{0x}}, \tag{2}$$

where v_e is the electron thermal velocity, c is the speed of light, k_s is the wave number of side-scattered light, and k_{0x} is the wave number of the pump wave in the direction of the density gradient (assumed to be the x axis), i.e., it takes into account the effect of an obliquely incident pump wave. It is seen that the values for the gain diverge in these formulas as the respective damping/electron temperature vanishes. Mostrom and Kaufman developed a more sophisticated model by considering the x-space Schrödinger equation to describe SRSS [14] (we refer to this model here as the x-space theory of SRSS), and they obtained a different scaling for convective gains. The gain is given by

$$\Gamma_s = 1.1\left(\frac{\omega_s}{\omega_0}\right)^{1/3}\left(\frac{\omega_s}{\omega_{pr}}\right)^{1/12}\frac{k_{br}^{3/2}a_0^{3/2}c^{1/2}L}{\omega_{pr}^{1/2}}, \tag{3}$$

where ω_0 is the pump frequency, k_{br} is the wave number of the Langmuir wave at the resonant point, a_0 is the normalized pump amplitude, and L is the density scale length. Note that the coefficient differs from the original one since the definition of the laser amplitude differs from ours (by a factor of 2 in a_0). However, the x-space theory is limited since both the thermal and damping terms are neglected. The $a_0^{3/2}$-scaling for the gain in Eq. (3) seems to be hard to reconcile with the a_0^2-scaling seen in both Eq. (1) and (2), and to date no one has shown the connection.

To settle this problem, and to better understand the behavior of SRSS in the convective regime, we have developed a k-space theory of SRSS. The real-space coupling equations for the decay waves are Fourier-transformed into k-ω space equations, which we call the k-space equations. A k-space Schrödinger equation is obtained by combining the two k-space equations characterizing the linear behavior of SRS. A Schrödinger equation with a quartic potential (in k-space) is seen to describe SRSS, while that with a quadratic potential describes backscattering. The Schrödinger equation can be solved through the use of the WKB approximation, and the convective gain is defined as the imaginary part of the phase integral, integrated from incident wave number to exit wave number [16]. It can be seen that side scatter is intrinsically different from back scatter since an eigenvalue exists in the Schrödinger equation with a quartic potential while it is absent in the quadratic potential (back scatter) case. We have shown that this eigenvalue in the wave number dramatically modifies the gain, with the maximum gain occurring not at the perfect matching condition but at a wave number with a small deviation that is associated with the eigenvalue. It appears that this phenomenon was first noticed by Short [17], but the introduction of a small mismatch in resonance was given without explanation. The origin of the mismatch is actually due to the eigenvalue effect, as proven here. Finally, all of the previously proposed formulas are compared and verified by numerical solutions of k-space equations. The k-space method has a long history, but it has been associated with the calculation of absolute instability thresholds [7,17–19]. We have shown here that the k-space theory is more generally useful than that.

The paper is organized as follows: Section II presents our k-space theory of SRSS and explains the nature of the Schrödinger equation that results. Section III describes the gain calculation, where previous results are reproduced unambiguously. In Sec. IV, we show that near the eigenvalues of SRSS the gain changes dramatically, and we derive the small wave-number deviation from the perfect resonance. We compare all these results with numerical solutions in Sec. V. Finally, the conclusions are demonstrated in Sec. VI.

II. THE k-SPACE THEORY OF SRS

We start with the linearized equations for SRS:

$$\left[\frac{\partial^2}{\partial t^2} + 2\nu_s\frac{\partial}{\partial t} - c^2\nabla^2 + \omega_{pr}^2\left(1+\frac{x}{L}\right)\right]\mathbf{a}_s = -\omega_{pr}^2 a_p \mathbf{a}_0,$$
$$\left[\frac{\partial^2}{\partial t^2} + 2\nu_p\frac{\partial}{\partial t} - 3v_e^2\nabla^2 + \omega_{pr}^2\left(1+\frac{x}{L}\right)\right]a_p = c^2\nabla^2(\mathbf{a}_s\cdot\mathbf{a}_0), \tag{4}$$

where a linearly varying density profile $n_e = n_{er}(1+x/L)$ is assumed, and $\omega_{pr} = \sqrt{4\pi n_{er}e^2/m}$ is the plasma frequency at resonant point (chosen to be $x=0$). The quantity $\mathbf{a}_0 = e\mathbf{A}_0/mc^2 = \frac{1}{2}a_0\hat{\mathbf{e}}_0 e^{i(\mathbf{k}_0\cdot\mathbf{x}-\omega_0 t)} + \text{c.c.}$ is the normalized amplitude of the plane pump laser with a fixed a_0, while $\mathbf{a}_s = e\mathbf{A}_s/mc^2$ and $a_p = \delta n_e/n_{er}$ are the normalized amplitudes of scattered light and a Langmuir wave, respectively. As before, c and v_e are the speed of light and electron thermal velocity. ν_s and ν_p are the temporal dampings of scattered light and a Langmuir wave, respectively.

To analyze these coupling equations, especially for side scattering, a Fourier transform in space and time is used,

$$\hat{a}_s(\mathbf{k}_s,\omega_s) = \hat{\mathbf{e}}_s\int a_s(\mathbf{x},t)e^{-i(\mathbf{k}_s\cdot\mathbf{x}-\omega_s t)}d\mathbf{x}dt,$$
$$\hat{a}_p(\mathbf{k}_b,\omega_b) = \int a_p(\mathbf{x},t)e^{-i(\mathbf{k}_b\cdot\mathbf{x}-\omega_b t)}d\mathbf{x}dt. \tag{5}$$

In our discussion, $\hat{\mathbf{e}}_s = \hat{\mathbf{e}}_0$, indicating that the polarization coupling is maximized, and without loss of generation we assume the pump laser is incident in the x-y plane and polarized along the z axis. The discussed Fourier modes, $\hat{a}_s$ and $\hat{a}_p$, satisfy the three-wave matching conditions, $\omega_0 = \omega_s + \omega_b$ and $\mathbf{k}_0 = \mathbf{k}_s + \mathbf{k}_b$. Fourier transforming Eq. (4) by using Eq. (5) and keeping the lowest-order coupling, we have the corresponding Fourier space or k-space coupling equations,

$$\frac{d\hat{a}_s}{dk_{sx}} = i\frac{L}{\omega_{pr}^2}D_l\hat{a}_s + i\frac{La_0}{2}\hat{a}_p^*,$$
$$\frac{d\hat{a}_p^*}{dk_{bx}} = -i\frac{L}{\omega_{pr}^2}D_p\hat{a}_p^* - i\frac{k_b^2c^2a_0L}{2\omega_{pr}^2}\hat{a}_s. \tag{6}$$

The derivatives come from the explicit linear dependence on x, where k_{sx} and k_{bx} are x components of $\mathbf{k}_s$ and $\mathbf{k}_b$. It is convenient to regard the resonant point as a reference point, therefore, according to the matching condition, k_{sx} and k_{bx} can be related to a new variable, $k = k_{sx} - k_{srx} = k_{brx} - k_{bx}$, where k_{srx} and k_{brx} are wave numbers at resonance. $k=0$ denotes the resonant point as shown in Fig. 1(a). With this

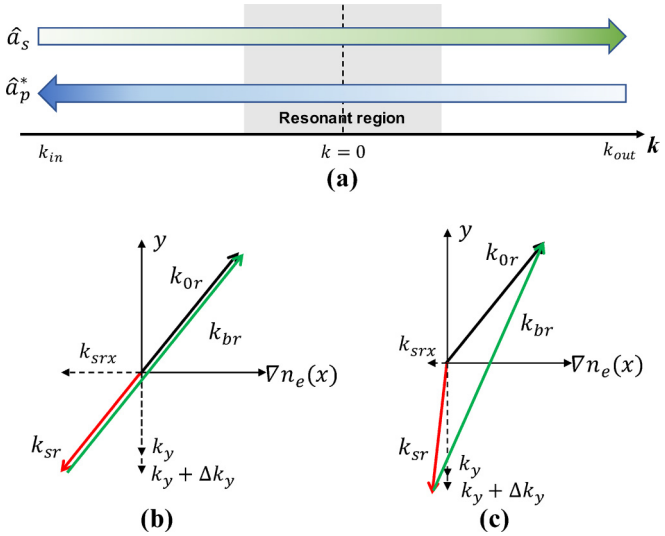

FIG. 1. (a) Interaction of waves in k-space. $k = 0$ represents the resonant point at $x = 0$. (b) Wave-number matching condition of back scatter at $k = 0$. (c) Wave-number matching condition of side scatter at $k = 0$. Obliquely incident pump (black arrow), scattered light (red arrow), and Langmuir wave (green arrow) are shown at the resonant point (subscript r). The scattered light wave number is decomposed into two directions, and in the perpendicular direction, a wave number deviation, Δk_y, from a perfect resonant condition is added to k_y.

definition, the k-space coupling equations reduce to

$$\frac{d\hat{a}_s}{dk} = i\frac{L}{\omega_{pr}^2} D_l \hat{a}_s + i\frac{La_0}{2}\hat{a}_p^*,$$
$$\frac{d\hat{a}_p^*}{dk} = i\frac{L}{\omega_{pr}^2} D_p \hat{a}_p^* + i\frac{k_b^2 c^2 a_0 L}{2\omega_{pr}^2}\hat{a}_s. \tag{7}$$

The fluid-type wave dispersion functions are given by

$$D_l(k) = -\omega_s^2 - 2i\nu_s\omega_s + c^2k_s^2 + \omega_{pr}^2,$$
$$D_p(k) = -\omega_b^2 + 2i\nu_p\omega_b + 3v_e^2k_b^2 + \omega_{pr}^2, \tag{8}$$

which are functions of k since $k_s^2 = (k_{srx} + k)^2 + k_{sy}^2$ and $k_b^2 = (k_{brx} - k)^2 + k_{by}^2$. Other quantities are regarded as constants. Since we are dealing with the convective regime of SRS and the density is stationary in time, frequencies are assumed to be real constants throughout.

Equations (7) are two first-order ODEs due to the linear density inhomogeneity. Neglecting the coupling terms on the right-hand side, the solution for each wave is the k-space representation of the Airy function. The coupling terms are significant only in the resonant region where $D_l \approx 0$ and $D_p \approx 0$ as shown in Fig. 1(a). On combining these two first-order ODEs by eliminating $\hat{a}_p^*$, we obtain a homogeneous second-order ODE. A standard procedure to obtain the Schrödinger equation is by using the transform

$$\hat{a}_s = W(k)\exp\left[\frac{iL}{2\omega_{pr}^2}\int^k [D_l(k') + D_p(k')]dk'\right]. \tag{9}$$

Then the coupling equations become a Schrödinger-type equation,

$$\frac{d^2W}{dk^2} + [F_0(k) - F_1(k)]W = 0, \tag{10}$$

where the potentials sorted by descending order of L are,

$$F_0(k) = \frac{L^2}{4\omega_{pr}^2}\left[(D_l - D_p)^2 + k_{br}^2 v_0^2 \omega_{pr}^2\right], \tag{11}$$
$$F_1(k) = \frac{iL}{2\omega_{pr}^2}\frac{d(D_l - D_p)}{dk}, \tag{12}$$

where $v_0 = a_0 c$ is the quiver velocity and k_b is approximated by k_{br}, the Langmuir wave number at resonance.

The complexity of potential comes from the function $D_l - D_p$, whose form varies according to the scattering geometry. Figures 1(b) and 1(c) show the wave-number matching conditions for back scatter and side scatter at the resonant point (whose quantities are denoted by the subscript r). Since $k_{sx} = k_{srx} + k$ and $k_{bx} = k_{brx} - k$, $D_l - D_p$ is given by

$$D_l - D_p = -\omega_s^2 + c^2[(k_{srx} + k)^2 + (k_y + \Delta k_y)^2] + \omega_b^2 - 3v_e^2\left[(k_{brx} - k)^2 + k_{bry}^2\right] - 2i(\nu_s\omega_s + \nu_p\omega_b). \tag{13}$$

Here, we introduce a free variable Δk_y which represents a wave number deviation in k_y. That aside, the dispersion relations $\mathrm{Re}[D_l] = 0$ and $\mathrm{Re}[D_p] = 0$ are satisfied,

$$\omega_s^2 = \omega_{pr}^2 + c^2\left(k_{srx}^2 + k_y^2\right),$$
$$\omega_b^2 = \omega_{pr}^2 + 3v_e^2\left[k_{brx}^2 + (k_y + k_{0ry})^2\right]. \tag{14}$$

As we will see later, Δk_y can be treated as an eigenvalue to the Schrödinger equation. If $\Delta k_y = 0$, there will be perfect wave-number matching at the resonant point (for side scatter we will always have a nonzero and complex eigenvalue, which will be discussed later). Substituting Eqs. (14) into Eq. (13), $D_l - D_p$ reduces to

$$D_l - D_p \approx c^2k^2 + \left(2c^2k_{srx} + 6v_e^2k_{brx}\right)k + 2c^2k_y\Delta k_y - 2i(\nu_s\omega_s + \nu_p\omega_b). \tag{15}$$

For backward scattering [Fig. 1(b)], k_{srx} is large compared with k in the resonant region and $k_{srx} \sim k_{brx}$. The quadratic and thermal terms are negligible, and Eq. (15) takes a more simplified form

$$D_l - D_p \approx 2c^2k_{srx}k + 2c^2k_y\Delta k_y - 2i(\nu_s\omega_s + \nu_p\omega_b), \tag{16}$$

which is a linear function of k. In contrast, for side scatter, which is 90° or near 90° to the density gradient [Fig. 1(c)], we have $k_{srx} \sim 0$. Equation (15) remains unchanged, being a quadratic function of k.

On substituting Eq. (16) into Eq. (10), we have a normalized Schrödinger equation for *backward* SRS,

$$\frac{d^2W}{dK_0^2} + [(K_0 + g_0 - i\nu_0)^2 + G_0 - i]W = 0, \tag{17}$$

where the normalized parameters are

$$K_0 = kl_b,$$
$$g_0 = \Delta k_y l_b \frac{k_y}{k_{srx}},$$

$$\nu_0 = \frac{(\nu_s\omega_s + \nu_p\omega_b)l_b}{c^2 k_{srx}},$$
$$G_0 = \frac{k_{br}^2 a_0^2 L}{4k_{srx}}. \tag{18}$$

A characteristic length for back scatter, $l_b = \frac{c\sqrt{k_{srx}L}}{\omega_{pr}}$, has also been defined. For *side scattering*, the normalized Schrödinger equation is given by

$$\frac{d^2W}{dK_1^2} + \left[\frac{1}{4}\left(K_1^2 + g_1 - i\nu_1\right)^2 + G_1 - iK_1\right]W = 0, \tag{19}$$

with a different normalization,

$$K_1 = \left(k + k_{srx} + \frac{3v_e^2}{c^2}k_{brx}\right)l_s,$$
$$g_1 = \left[2k_y\Delta k_y - \left(k_{srx} + \frac{3v_e^2}{c^2}k_{brx}\right)^2\right]l_s^2,$$
$$\nu_1 = \frac{2(\nu_s\omega_s + \nu_p\omega_b)l_s^2}{c^2},$$
$$G_1 = \frac{k_{br}^2 a_0^2}{4}\left(\frac{L^2 c}{\omega_{pr}}\right)^{2/3}. \tag{20}$$

The characteristic length for side scatter, $l_s = (\frac{c^2 L}{\omega_{pr}^2})^{1/3}$, differs from that for back scatter. It is seen that $l_s \ll l_b$ while $G_1 \gg G_0$ for the conditions with large density scale length L.

The two Schrödinger equations, Eqs. (17) and (19), in the variable k characterize the properties of a range of SRS geometries. The potential is essentially a quadratic function of k for backward scattering or a quartic function of k for side scattering. Physically speaking, these potentials, both having a positive coefficient of second or fourth order, belong to the physics of underdense barriers. At the core of such scattering problems is the scattering rate of an outgoing wave interacting with these potentials. The ratio of the amplitudes, integrated from k_{in} to k_{out}, determines the scattering rate, and its exponential index denotes the gain. Here, we define stable scattering as the case with a scattering rate (or gain) that changes little with the deviation from perfect matching, Δk_y (or g), while an unstable scattering is one where the scattering rate (or gain) changes dramatically with Δk_y (or g). As will be discussed later, backward scattering (with the quadratic potential) is stable scattering, and side scattering (with the quartic potential) belongs to an unstable scattering type. This is a fundamental property of the scattering type of solutions to Schrödinger equations. The determination of this nature and its consequence in k-space for SRS is one of the noteworthy results of this work.

Dating back to the very beginning of the studies on laser plasma instabilities, we find that these two types of potential were first discovered by Rosenbluth [20] from an x-space theory of the coupling envelope equations. Absolute instability, characterized by a temporal growth rate, only exists in the quartic potential. However, the x-space Schrödinger equation with a quartic potential is not able to describe SRSS, since the envelope equation fails for SRSS, and the potential function in x-space is much more complicated than a quartic function [14].

III. GAIN CALCULATION BY THE WKB METHOD

The solution of the Schrödinger equations with initial conditions is the key to understanding the initial behavior of SRS. Equation (17) reduces to the well-known parabolic cylinder equation whose exact solutions are fully understood [21]. However, for Eq. (19), which describes side scatter, no exact solutions have been found. Therefore, the Wentzel-Kramers-Brillouin (WKB) approximation is used to construct approximate solutions for the Schrödinger equations.

Such solutions can be written by $W(K) = \frac{A_+}{F(K)^{1/4}}e^{i\int^K\sqrt{F(K')}dK'} + \frac{A_-}{F(K)^{1/4}}e^{-i\int^K\sqrt{F(K')}dK'}$ when turning points of $F(K)$ are not encountered, i.e., $F(K) = 0$. Here, $F(K)$ denotes the potential in Eqs. (17) and (19), and A_+, A_- are arbitrary constants determined by initial conditions. The WKB solutions are used to describe incoming and outgoing waves, and the imaginary part of the phase integral $\int^K\sqrt{F(K')}dK'$ characterizes the *spatial* growth of the wave. Therefore, the convective gain is defined by

$$G = \left|\text{Im}\left[\int_{-\infty}^{\infty}\sqrt{F(K)}dK\right]\right|. \tag{21}$$

Note that the upper and lower limits of the integral should be finite in reality due to the effect of finite inhomogeneity or finite beam width. Here, we assume that k_{in} and k_{out} are much larger than the characteristic length of the resonant region, as shown in Fig. 1(a), so that the limits can be extended to infinity. The effect of finite beam width or plasma length will be discussed elsewhere. To evaluate the integral, a Stokes diagram for the integrand is a useful tool [16].

First, let us begin with the well-understood case of backward scattering from our new k-space perspective. Assuming $G_0 \gg 1$, we neglect the constant i in the potential, and then the integral becomes

$$G = \left|\text{Im}\left[\int_{-\infty}^{\infty}\sqrt{(K_0 + g_0 - i\nu_0)^2 + G_0}dK_0\right]\right|. \tag{22}$$

Its Stokes diagram is shown in Fig. 2(a). As long as the imaginary part of $g_0 - i\nu_0$ is not too large, we can easily obtain the convective gain for backward scattering by integrating along the red arrows. Since along an anti-Stokes line [solid curve in Fig. 2(a)] the imaginary part vanishes, the integral is just performed between two turning points,

$$G = 2G_0\int_{\arcsin(|\nu_0 - \text{Im}[g_0]|/\sqrt{G_0})}^{\pi/2}\cos^2\theta d\theta. \tag{23}$$

When $\nu_0 = g_0 = 0$, it recovers the familiar Rosenbluth gain,

$$G = \pi G_0/2 = \frac{\pi k_{br}^2 a_0^2 L}{8k_{srx}} \equiv G_{\text{Ros}}. \tag{24}$$

The integral is slowly affected by the lower limit as long as $|\nu_0 - \text{Im}[g_0]| \ll \sqrt{G_0}$. It shows that the convective gain of backward scattering is weakly dependent on the deviation (mismatch) g_0, implying that backward scattering is *stable*in the sense that we have previously defined.

For side scattering, the phase integral becomes much more complicated. To begin with, we discuss the case of $g_1 = 0$, i.e., perfect resonance at the turning point. The integral can be evaluated in two limits. First, in the limit of weak damping,

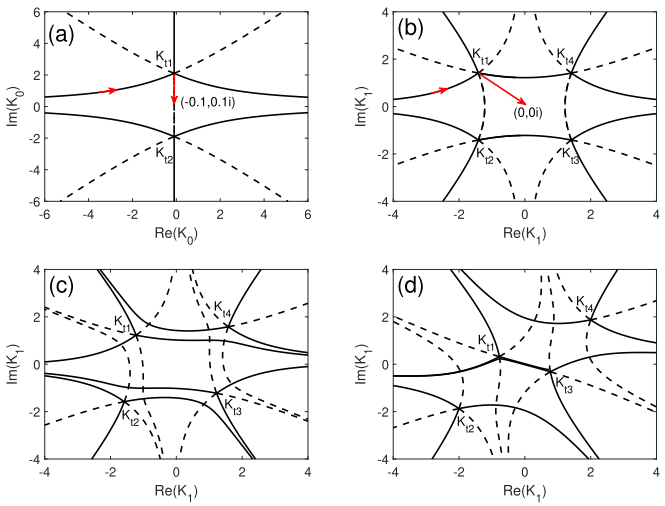

FIG. 2. Stokes diagrams for the potential $F(K)$ in four limiting cases: (a) Back scatter: $F(K_0) = (K_0 + 0.1 - 0.1i)^2 + 4$; (b) side scatter: $F(K_1) = K_1^4/4 + 4$; (c) side scatter: $F(K_1) = (K_1^2 - i)^2/4 + 4$; (d) side scatter at an eigenvalue: $F(K_1) = (K_1^2 - 0.5 - 3.5i)^2/4 + 4$. The solid line is the anti-Stokes line defined as $\mathrm{Im}[\int^K \sqrt{F(K')}dK' = 0]$, and the dashed line is the Stokes line defined as $\mathrm{Re}[\int^K \sqrt{F(K')}dK' = 0]$.

$\nu_1 \ll 1$,

$$G = \left|\mathrm{Im}\left[\int_{-\infty}^{\infty} \sqrt{K_1^4/4 + G_1}dK_1\right]\right|. \tag{25}$$

The Stokes diagram is shown in Fig. 2(b), and the deformed contour is shown by the red arrows. Along the contour we have

$$\mathrm{Im}\int_{-\infty}^{\infty} \sqrt{K_1^4/4 + G_1}dK_1 = 2\,\mathrm{Im}\int_{K_{t1}}^{0} \sqrt{K_1^4/4 + G_1}dK_1 = 1.748 G_1^{3/4}.$$

The convective gain is thus given by

$$G = 1.748\, G_1^{3/4} = 0.618\frac{k_{br}^{3/2} a_0^{3/2} c^{1/2} L}{\omega_{pr}^{1/2}}. \tag{26}$$

Comparing this with Eq. (3) (the convective gain proposed by Mostrom and Kauffman), we see that it has the same scaling (and in particular $\sim a_0^{3/2}$) but the coefficient is slightly different.

As the damping increases, the turning points become asymmetric. Two diagonal turning points shrink inward, while the other two stretch out as shown in Fig. 2(c). The integral can be simplified in the limit of strong damping, $\nu_1 \gg 1$, by using the Taylor expansion,

$$\mathrm{Im}\int_{-\infty}^{\infty} \sqrt{\frac{1}{4}\left(K_1^2 - i\nu_1\right)^2 + G_1}dK_1 \approx \mathrm{Im}\int_{-\infty}^{\infty} \frac{1}{2}\left(K_1^2 - i\nu_1\right)dK_1 + \mathrm{Im}\int_{-\infty}^{\infty} \frac{G_1}{K_1^2 - i\nu_1}dK_1.$$

The first term is connected with damping mitigation, while the second term represents a type of path integral in the k-space [a general form of this path integral formula is given by Eq. (A3) in Appendix]. We evaluate this term

$$\mathrm{Im}\int_{-\infty}^{\infty} \frac{G_1}{K_1^2 - i\nu_1}dK_1 = \int_{-\infty}^{\infty} \frac{G_1\nu_1}{K_1^4 + \nu_1^2}dK_1 = \frac{\pi G_1}{\sqrt{2\nu_1}}.$$

This result is actually the same as the gain derived by Michel *et al.* from a path integral method [3], but now generalized to include damping of the scattered light wave,

$$G = \frac{\pi G_1}{\sqrt{2\nu_1}} = G_{\mathrm{Ros}}(0)\frac{k_{sr}c}{\sqrt{\nu_s\omega_s + \nu_p\omega_b}}. \tag{27}$$

The above is exactly Eq. (1) when $\nu_s = 0$. Equation (2) of Michel *et al.* [3] is also attainable under some conditions (see Appendix). A proof of the equivalence between the k-space theory and this path integral method is also presented in Appendix, which is a new result as no proof was given by Michel *et al.* [3].

IV. THE k-SPACE EIGENVALUES OF SRSS AND THE CONSEQUENCES FOR GAIN MODIFICATION

When g_1 is included in Eq. (19) for the Schrödinger equation with a quartic potential, the physical results change qualitatively. Figure 2(d) shows the Stokes diagram for a specific value of g_1. Two turning points are very close to the real axis, and an anti-Stokes line (along which the amplitude $|W|$ is constant, i.e., a purely oscillatory solution) connects them. This makes the system look like a quantum harmonic oscillator where an eigenvalue inherently emerges. Moreover, since the turning points are near the contour of integration, the WKB approximation is no longer valid, and the gain must be calculated numerically.

Therefore, the physics of side scattering is essentially an eigenvalue problem, even when one is dealing with the convective regime. The quantity g_1 acts as an eigenvalue that determines the eigenstate for side scatter. As is well known, if g_1 is an undetermined quantity in frequency, the solution of the Schrödinger equation with vanishing boundary condition requires a complex eigenvalue. When $\mathrm{Im}[g_1] > 0$, an absolute instability emerges [7,17]. But here, g_1 is an eigenvalue in wave number, and not temporal frequency. This eigenvalue will affect the convective growth of SRSS.

Similar to what has been done in Rosenbluth's seminal paper [20], the eigenvalue in wave number is derived as follows: Assume G_1 is large enough so that we neglect the effect of iK_1 in the integral. The four complex turning points of the quartic potential are $K_t = \sqrt{\pm 2i\sqrt{G_1} + i\nu_1 - g_1}$. We assume

$$g_1 = -2i\sqrt{G_1}(1 - \delta) + i\nu_1, \tag{28}$$

where $\delta \ll 1$, such that turning points close to the real axis of K_1 exist. Then the quartic potential reduces to

$$F(K_1) \approx \tfrac{1}{4}\left(K_1^2 + 2i\delta\sqrt{G_1}\right)\left(K_1^2 - 4i\sqrt{G_1}\right). \tag{29}$$

For an eigenvalue problem, the eigenvalue should satisfy the Bohr-Sommerfeld quantization condition, $\int_{K_{t1}}^{K_{t3}} \sqrt{F(K_1)}dK_1 = (n + \frac{1}{2})\pi$, where $n = 0, 1, 2, \ldots$. Substituting Eq. (29) into the quantization condition and noting that $K_1^2 \ll 4i\sqrt{G_1}$, the integral on the left-hand side is readily obtained, $\int_{K_{t1}}^{K_{t3}} \sqrt{F(K_1)}dK_1 = \sqrt{-i}\pi G_1^{3/4}\delta$. Then we

have

$$\delta = \left(n + \frac{1}{2}\right) G_1^{-3/4} e^{i\pi/4}. \tag{30}$$

The eigenvalue in *wave number* is thus obtained,

$$g_n = -\frac{\sqrt{2}\left(n+\frac{1}{2}\right)}{G_1^{1/4}} + 2i\sqrt{G_1}\left(\frac{n+\frac{1}{2}}{\sqrt{2}G_1^{3/4}} - 1\right) + iv_1. \tag{31}$$

The subscript n means the nth eigenvalue of g_1. This is a normalized eigenvalue, expressed by a function of Δk_y. It can also be transformed into an eigenvalue in *frequency* if we express the frequency in Eq. (8) as $\omega_s \to \omega_s + \Delta\omega$, $\omega_b \to \omega_b - \Delta\omega$, and neglect Δk_y. The equivalency shows that $-2\omega_0\Delta\omega/c^2 = 2k_y\Delta k_y$. After normalization, the growth rate, defined by $\gamma = \mathrm{Im}[\Delta\omega]$, is $\gamma = -\mathrm{Im}[g_n]c^2/2\omega_0 l_s^2$, which is consistent with that derived by Afeyan and Williams [7] (except for a small correction). It shows that $\mathrm{Im}[g_n] = 0$ corresponds to the absolute threshold of SRSS.

To understand how the wave-number deviation affects the convective gain of SRSS, we numerically solve the coupling equations in k-space [Eq. (7)] and use an outgoing wave boundary condition, $\hat{a}_s(k_{\mathrm{out}}) = 1$ and $\hat{a}_p^*(k_{\mathrm{out}}) = 0$, where k_{out} is the x-component of the scattered wave number at vacuum. As shown in Fig. 1(a), the integration along the real k axis, inbound from the vacuum to the resonant point and back to the vacuum, gives us the required metric in order to calculate the convective gain, $G = \ln(|\hat{a}_s(k_{\mathrm{out}})|/|\hat{a}_s(k_{\mathrm{in}})|)$ [17].

Figure 3(a) shows the typical solutions of $|\hat{a}_s|$ in k-space. Interaction occurs only in the resonant region $k \sim 0$ (damping of scattered light is ignored for simplicity). The black curve represents the solution of backward scattering, and the red curve shows the side scattering with a real and negative wave-number deviation. The localized oscillatory structure of side scattering is actually the eigenstate structure, and the number of periods indicates the order of the eigenstate. As we change g_1 continuously (g_1 must be a real number because of its physical meaning), the period is changed accordingly, leading to a dramatic bouncing of the output amplitude level, however there are no oscillations for the backward scattering as g_0 changes.

With the numerical convective gain is defined by $G = \ln(|\hat{a}_s(k_{\mathrm{out}})|/|\hat{a}_s(k_{\mathrm{in}})|)$, we plot the dependence of gain on the wave-number deviation in Fig. 3(b). As shown, the gain for backward scattering is almost independent of Δk_y (or g_0), which means backward scattering is a stable scattering. However, the gain for side scattering oscillates dramatically due to the eigenvalue effect. This illustrates how the wave-number deviation can affect the convective gain of SRSS, and it is undoubtedly an unstable scattering.

Since the real-space behavior is a summation over all modes in k space, the one with the maximum gain will also dominate in the real space. We observe that the maximum gain of SRSS is located on the lowest order eigenmode, *and not the perfect resonant mode* ($\Delta k_y = 0$), and the real part of the eigenvalue determines the wave-number deviation from the perfect resonance,

$$\Delta k_y = \frac{1}{2k_y}\left(k_{srx} + \frac{3v_e^2}{c^2}k_{brx}\right)^2 - \frac{\omega_{pr}^{3/2}}{2k_y k_{br}^{1/2} a_0^{1/2} c^{3/2} L}. \tag{32}$$

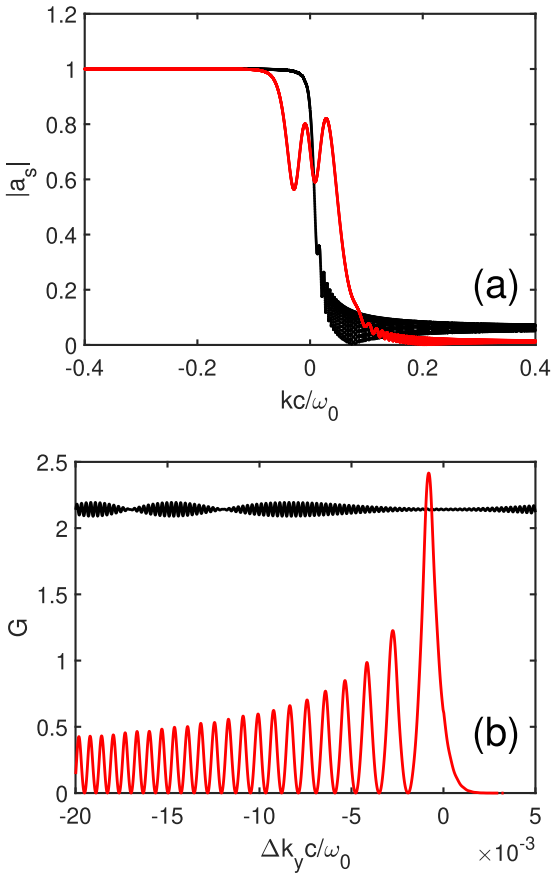

FIG. 3. (a) Typical numerical solutions of the k-space coupling equation [Eq. (7)] for back scattering (black curve) and side scattering (red curve). (b) Convective gain as a function of wave-number deviation Δk_y for back scattering (black curve) and side scattering (red curve). The gain is evaluated by $G = \ln(|\hat{a}_s(k_{\mathrm{out}})|/|\hat{a}_s(k_{\mathrm{in}})|)$.

For the numerical case shown in Fig. 3(b), we find that with $k_{srx} = 0$ the real deviated wave number is $\Delta k_y = -7.9 \times 10^{-4}\omega_0/c$, which is close to our theoretical prediction, $\Delta k_y = -9.4 \times 10^{-4}\omega_0/c$. We can also expect a perfect match ($\Delta k_y = 0$) as long as the longitudinal wave number can compensate for the deviation,

$$k_{srx} = -\frac{3v_e^2}{c^2}k_{brx} + \frac{\omega_{pr}^{3/4}}{k_{br}^{1/4} a_0^{1/4} c^{3/4} L^{1/2}}. \tag{33}$$

We note that in a recent paper, Short [17] has also observed the phenomenon of gain modification, but he did not give an explanation for this phenomenon—as we now do here. The inherent shift of the phase matching condition is innate in an eigenvalue problem such as SRSS and it can affect the gain dramatically. However, no analytic formula can predict the maximum gain modified by the eigenvalue, hence it must be calculated numerically.

V. NUMERICAL VERIFICATION: COMPARISONS BETWEEN NUMERICAL AND THEORETICAL GAINS

In this section, we compare all the formulas that have been proposed with numerical solutions to the k-space equations for side scattering. In doing so, we determine which

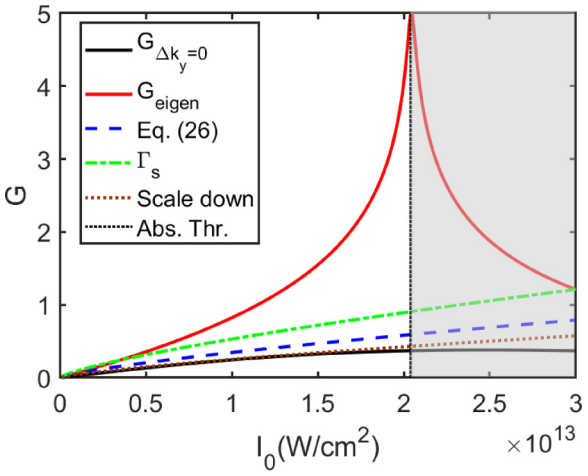

FIG. 4. Gain comparison without damping. Numerical parameters are $\lambda_0 = 0.351$ μm, $L = 500$ μm, $\theta_0 = 50°$, $n_{er} = 0.175n_c$, and $T_e = 0$ keV. The shaded area is dominated by absolute instability (positive eigenvalue in frequency), and convective gains are no longer valid here.

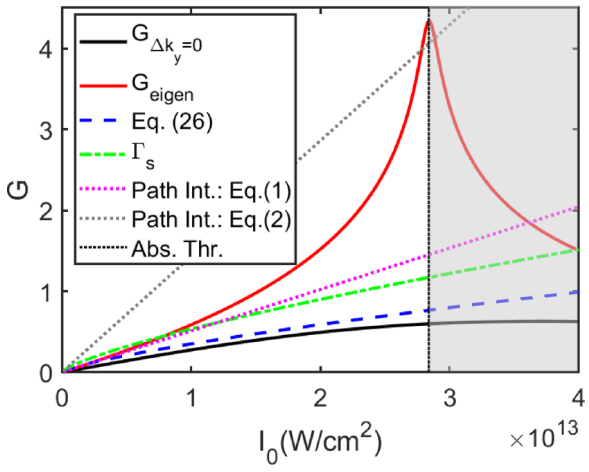

FIG. 5. Gain comparison with small damping. Numerical parameters are $\lambda_0 = 0.351$ μm, $L = 500$ μm, $\theta_0 = 50°$, $n_{er} = 0.17n_c$, and $T_e = 1$ keV. The corresponding dampings are $\nu_{ei} = 2.2 \times 10^{-4}\omega_0$ and $\nu_{\rm LD} = 1.8 \times 10^{-11}\omega_0$. The shaded area is dominated by absolute instability (positive eigenvalue in frequency), and convective gains are no longer valid here.

formulas are better able to predict the severity of SRSS, and which are of practical utility (e.g., for implementation in ICF ray-tracing codes, for example).

First, let us assume that damping is negligible, i.e., $\nu_s = 0$ and $\nu_p = 0$. Therefore, the formulas from the path integral method [Eqs. (1), (2), or (27)] are not appropriate. Only the formula derived by Mostrom [Eq. (3)] and by us [Eq. (26)] by the WKB method are valid. Recall that the two only differ by the coefficient.

Figure 4 shows the gains for the case of (backward) side scatter for an obliquely incident pump [see Fig. 1(c)] as a function of laser intensity. (Note that "backward" here refers to the projection of the side scattered light wave vector onto that of the obliquely incident pump.) The numerical parameters are $\lambda_0 = 0.351$ μm, $L = 500$ μm, $\theta_0 = 50°$, $n_{er} = 0.175n_c$, and $T_e = 0$ keV. The solid lines are numerical results where the gain without wave-number deviation is shown in black and the maximum gain of the lowest eigenstate is shown in red. As seen in Fig. 3, when g_1 approaches the eigenvalue, the gain increases dramatically. This explains the gap between two solid curves. When the imaginary part of the eigenvalue vanishes [Eq. (31)] as we increase the intensity, g_1 exactly equals the eigenvalue, which as expected would lead to a vanishing $\hat{a}_s(k_{\rm in})$, or infinite gain. Therefore, a sharp peak emerges, in the plots, for intensities beyond which absolute instability is present and convective gain ceases to have any physical meaning. Mathematically, for intensities beyond the threshold intensity, g_1 becomes far from the eigenvalue and the gain decreases.

Notice that if we consider the eigenvalues in both wave number and frequency together, we find that below the absolute threshold, the eigenvalue in frequency has a negative imaginary part, leading to an exponentially decaying temporal solution, but the eigenvalue in wave number gives rise to convective growth. Therefore, below the absolute threshold, it is dominated by convective growth. Above the absolute threshold, convective growth weakens and positive temporal growth dominates. The instability here becomes absolutely unstable in the shaded region shown in Fig. 4. Therefore, this peak provides a way to calculate the absolute threshold [17,22].

A comparison between the curves shows that the gain obtained from the WKB method (blue-dashed line) is closer to $G_{\Delta k_y=0}$ than that from Mostrom and Kaufman (green dash-dotted line), but none of the formulas are able to match $G_{\rm eigen}$. One may think Mostrom's gain seems good at the very beginning of $G_{\rm eigen}$. However, that is not true because the scalings are quite different: If we scale Eq. (26) or (3) slightly (the coefficient changes from 0.618 to 0.45), it can be made to perfectly match $G_{\Delta k=0}$, as shown in the brown-dotted line. This means that Eq. (3) is more likely to predict the noneigenmode gain, but it is not as good as our WKB result. This can also be checked in the following examples. The small discrepancy between Eq. (26) and $G_{\Delta k_y=0}$ is just due to the finite integration limit.

Next, we add a small damping to the wave coupling system so that the gains from the path integral method can be compared. The parameters discussed here are more realistic, $\lambda_0 = 0.351$ μm, $L = 500$ μm, $\theta_0 = 50°$, $n_{er} = 0.17n_c$, and $T_e = 1$ keV (which corresponds to a scattered light wavelength $\lambda_s = 609$ μm). The damping rates here are not large—collisional damping is $\nu_{ei} = 2.2 \times 10^{-4}\omega_0$ and Landau damping is $\nu_{\rm LD} = 1.8 \times 10^{-11}\omega_0$.

Figure 5 shows the gain comparison with small damping. Again, a sharp peak exists for $G_{\rm eigen}$, determining the absolute threshold, and Eq. (26) is close to $G_{\Delta k_y=0}$. The two path integral formulas perform differently. As shown by the gray-dotted line, Eq. (2), which includes thermal effects, does not predict the numerical gains well, even if we further increase the electron temperature. However, the damping-dominated gain in the dotted-purple line derived from the path integral [Eq. (1)] or the k-space integral [Eq. (27)] is surprisingly good at predicting $G_{\rm eigen}$ at the beginning, although the gap between the predictions of Eq. (1) and $G_{\rm eigen}$ increases quite dramatically as the absolute threshold is approached. Some

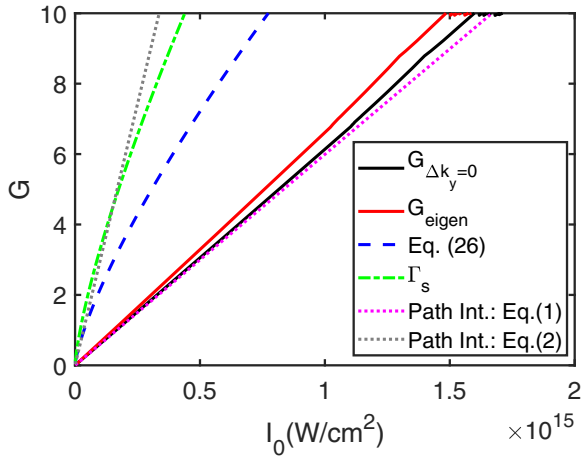

FIG. 6. Gain comparison with strong damping. Numerical parameters are $\lambda_0 = 0.351$ μm, $L = 500$ μm, $\theta_0 = 50°$, $n_{er} = 0.14n_c$, and $T_e = 5$ keV. The corresponding damping rates are $\nu_{ei} = 2.1 \times 10^{-5}\omega_0$ and $\nu_{\rm LD} = 0.017\omega_0$.

extended discussions on the applicability conditions of these two formulas are presented in Appendix.

If we further increase the wave damping rates by increasing the electron temperature to $T_e = 5$ keV and the resonant density to $n_{er} = 0.14n_c$ ($\lambda_s = 620$ μm), the collisional and Landau damping are, respectively, $\nu_{ei} = 2.1 \times 10^{-5}\omega_0$ and $\nu_{\rm LD} = 0.017\omega_0$. The gain comparison shown in Fig. 6 indicates that only Eq. (1) or (27) can accurately predict the numerical gains in this strong damping regime. This is because the size of the resonant region increases with increased damping. When the size of the resonant region increases, the effect of the eigenvalue becomes less and less important. When the eigenmode is unimportant, the WKB approximation is good enough to accurately predict the gain. The imaginary part of the eigenvalue g_1 is negligible compared with the damping ν_1, so the black curve and red curve are close to each other. For this reason, the intensity scaling law becomes linear, $G \propto I$, as with the case of backward scattering. There is also an absolute threshold in this case, but the threshold intensity is as high as 10^{15} W/cm^2, and the gain above that threshold becomes chaotic (see Ref. [22]), which is not shown here. To summarize, in this strong damping regime, the path integral method gives reasonably accurate results.

VI. CONCLUSIONS

In this paper, we have developed a k-space theory of SRS. The linearized SRS equations in k-space can be described by two types of Schrödinger equation. The Schrödinger equation with a quadratic potential characterizes backward SRS, while the Schrödinger equation with a quartic potential describes side scattering, where the scattered light is nearly perpendicular to the local density gradient. We have also built connections of k-space theory with the existing x-space theory and a simpler path integral method (with details in the Appendixes). A similar k-space path integral formula is derived in Eq. (A3).

The k-space theory is used to calculate the convective gains of SRSS in order to clarify some misunderstandings on the gain of SRSS. The WKB solutions of Schrödinger equations reproduce the Rosenbluth gain for backward or oblique scattering and give us better gain predictions for SRSS in two limits: Eq. (26) for the weak damping limit, and Eq. (27) for the strong damping limit. However, SRSS is essentially an eigenvalue problem. The eigenvalue can dramatically modify the gain, which cannot be correctly predicted by the WKB method. We term this an unstable scattering problem, compared with stable scattering such as backward scattering. We find that the maximum gain occurs not at the perfect matching condition but with a small wave-number deviation correlated with the real part of the eigenvalue of SRSS.

Numerical solutions of k-space coupling equations consolidate these perspectives and show us how to correctly use the different gain formulas and to assess the severity of SRSS for given interaction conditions. When damping is negligible, Eq. (26) can better predict the gain at perfect resonance ($\Delta k_y = 0$). However, the maximum gain should be evaluated numerically due to modifications caused by the eigenvalue. As damping starts to dominate the regime, the path integral formula, Eq. (27) or Eq. (1), becomes more and more accurate. The eigenvalue effect fades away gradually, leaving the system more likely to behave as backward scattering—which can be considered as a smooth transition to what we are familiar with.

ACKNOWLEDGMENTS

We are grateful for the discussions with R. Fedosejevs. This work was supported by the Strategic Priority Research Program of Chinese Academy of Sciences (Grant No. XDA25050700), National Natural Science Foundation of China (Grant No. 11805062), and Natural Science Foundation of Hunan Province, China (Grant No. 2020JJ5029). This work is funded by China Scholarship Council. J.F.M. and Q.W. acknowledge the support of the Natural Sciences and Engineering Research Council of Canada (NSERC) (funding reference numbers RGPIN-2018-05787, RGPAS-2018-522497).

APPENDIX: CONNECTIONS BETWEEN THE k-SPACE THEORY AND THE PATH INTEGRAL METHOD

In this Appendix, we show that we can obtain a gain formula, involving a k-space path integral, that reproduces Eqs. (1) and (2) as previously derived by Michel *et al.* [3] from the k-space theory.

The path integral method is used to obtain a convective gain by integrating the coupling coefficient along the trajectory of the scattered light ray. The integral is derived from x-space steady-state intensity coupling equations, under the assumption of strong damping. The method is very appealing as it can be easily combined with ray-tracing codes to quickly assess the severity of SRS instability due to its simplicity [23]. The path integral formula often has a form of [3]

$$G = \int_S \frac{k_b^2 a_0^2 \omega_{pr}^2}{8k_s} \frac{2\nu_p \omega_b}{D(s)^2 + 4\nu_p^2 \omega_b^2} ds, \tag{A1}$$

where G is modified to amplitude gain, and $D(s)$ is the real part of the Langmuir wave dispersion function.

This type of integral is also attainable from the k-space theory. Without loss of generality, we use the dimensional form of Eqs. (10)–(12) to derive the path integral formula in k-space. Since strong damping is assumed, we can Taylor expand the phase integral:

$$\begin{aligned} G &= \mathrm{Im}\left[\frac{L}{2\omega_{pr}^2}\int^k \sqrt{(D_l-D_p)^2+k_{br}^2v_0^2\omega_{pr}^2}dk'\right] \\ &\approx \mathrm{Im}\left[\frac{L}{2\omega_{pr}^2}\int^k (D_l-D_p)\left(1+\frac{k_{br}^2v_0^2\omega_{pr}^2}{2(D_l-D_p)^2}\right)dk'\right] \\ &= \mathrm{Im}\left[\frac{L}{2\omega_{pr}^2}(D_l-D_p)k\right]+\mathrm{Im}\left[\frac{L}{4\omega_{pr}^2}\int^k \frac{k_{br}^2v_0^2\omega_{pr}^2}{D_l-D_p}dk'\right]. \end{aligned} \tag{A2}$$

The approximation is valid when $k_{br}^2v_0^2\omega_{pr}^2 \ll (D_l-D_p)^2$. The first term relates to the mitigation effect (in k-space) of wave damping, and the second term is what we are seeking,

$$\begin{aligned} G_{\mathrm{path}} &= \mathrm{Im}\left[\frac{L}{4\omega_{pr}^2}\int^k \frac{k_{br}^2v_0^2\omega_{pr}^2}{D_l-D_p}dk'\right] \\ &= \frac{k_{br}^2v_0^2L}{4}\int^k \frac{2(\nu_p\omega_b+\nu_s\omega_s)}{(\mathrm{Re}[D_l-D_p])^2+4(\nu_p\omega_b+\nu_s\omega_s)^2}dk', \end{aligned} \tag{A3}$$

which has the same form as Eq. (A1).

It is easy to check this result. When backward scattering is considered, we have $D_l \approx 2c^2k_{sr}k - 2i\nu_s\omega_s$ and $D_p \approx -6v_e^2k_{br}k + 2i\nu_p\omega_b$. Substituting these into Eq. (A3), we obviously obtain the Rosenbluth gain, $G_{\mathrm{path}} = G_{\mathrm{Ros}}$, if k is integrated from $-\infty$ to ∞.

It is a little more complicated when we are dealing with side scattering. Without wave-number deviation, the dispersion relations are $D_l \approx c^2k^2 - 2i\nu_s\omega_s$ and $D_p \approx -6v_e^2k_{0x}k + 2i\nu_p\omega_b$. Substituting these into Eq. (A3), we have

$$G_{\mathrm{path}} = \frac{k_{br}^2v_0^2L}{4}\int^k \frac{2(\nu_p\omega_b+\nu_s\omega_s)}{\left(c^2k^2+6v_e^2k_{0x}k\right)^2+4(\nu_p\omega_b+\nu_s\omega_s)^2}dk'. \tag{A4}$$

The magnitudes of c^2k^2 and $6v_e^2k_{0x}k$ do affect the gain. For two limiting cases, we can obtain simple formulas. First, if $c^2k^2 \ll 6v_e^2k_{0x}k$, i.e., in the high-temperature regime, Eq. (A4) reduces to

$$G_{\mathrm{path}} = G_{\mathrm{Ros}}\frac{k_sc^2}{3v_e^2k_{0x}}, \tag{A5}$$

which is exactly Eq. (2). In the other limit, $c^2k^2 \gg 6v_e^2k_{0x}k$, i.e., in the low-temperature regime, Eq. (A4) reduces to

$$G_{\mathrm{path}} = G_{\mathrm{Ros}}\frac{k_{sr}c}{\sqrt{\nu_p\omega_b+\nu_s\omega_s}}, \tag{A6}$$

which is equivalent to Eq. (1).

[1] M. J. Rosenberg, A. A. Solodov, J. F. Myatt, W. Seka, P. Michel, M. Hohenberger, R. W. Short, R. Epstein, S. P. Regan, E. M. Campbell *et al.*, Phys. Rev. Lett. **120**, 055001 (2018).

[2] M. J. Rosenberg, A. A. Solodov, W. Seka, R. K. Follett, J. F. Myatt, A. V. Maximov, C. Ren, S. Cao, P. Michel, M. Hohenberger *et al.*, Phys. Plasmas **27**, 042705 (2020).

[3] P. Michel, M. J. Rosenberg, W. Seka, A. A. Solodov, R. W. Short, T. Chapman, C. Goyon, N. Lemos, M. Hohenberger, J. D. Moody, S. P. Regan, and J. F. Myatt, Phys. Rev. E **99**, 033203 (2019).

[4] G. Cristoforetti, L. Antonelli, D. Mancelli, S. Atzeni, F. Baffigi, F. Barbato, D. Batani, G. Boutoux, F. D'Amato, J. Dostal *et al.*, High Power Laser Sci. Eng. **7**, e51 (2019).

[5] C. Z. Xiao, H. B. Zhuo, Y. Yin, Z. J. Liu, C. Y. Zheng, Y. Zhao, and X. T. He, Plasma Phys. Controlled Fusion **60**, 025020 (2018).

[6] C. S. Liu, M. N. Rosenbluth, and R. B. White, Phys. Fluids **17**, 1211 (1974).

[7] B. B. Afeyan and E. A. Williams, Phys. Fluids **28**, 3397 (1985).

[8] R. P. Drake, R. E. Turner, B. F. Lasinski, K. G. Estabrook, E. M. Campbell, C. L. Wang, D. W. Phillion, E. A. Williams, and W. L. Kruer, Phys. Rev. Lett. **53**, 1739 (1984).

[9] R. P. Drake, R. E. Turner, B. F. Lasinski, E. A. Williams, D. W. Phillion, K. G. Estabrook, W. L. Kruer, E. M. Campbell, K. R. Manes, J. S. Hildum, and T. W. Johnston, Phys. Fluids **31**, 3130 (1988).

[10] R. P. Drake, Phys. Fluids B **1**, 1082 (1989).

[11] X. Zhao, X. H. Yuan, J. Zheng, Y. F. Dong, K. Glize, Y. H. Zhang, Z. Zhang, and J. Zhang, Rev. Sci. Instrum. **93**, 053505 (2022).

[12] R. P. Drake, E. A. Williams, P. E. Young, K. Estabrook, W. L. Kruer, D. S. Montgomery, H. A. Baldis, and T. W. Johnston, Phys. Fluids B **1**, 2217 (1989).

[13] S. Depierreux, C. Neuville, C. Baccou, V. Tassin, M. Casanova, P.-E. Masson-Laborde, N. Borisenko, A. Orekhov, A. Colaitis, A. Debayle *et al.*, Phys. Rev. Lett. **117**, 235002 (2016).

[14] M. A. Mostrom and A. N. Kaufman, Phys. Rev. Lett. **42**, 644 (1979).

[15] M. A. Mostrom, D. R. Nicholson, and A. N. Kaufman, Lawrence Berkeley Laboratory Report No. 2082, 1978 (unpublished).

[16] J. Heading, *An Introduction to Phase Integral Methods* (Methuen, London, 1962).

[17] R. W. Short, Phys. Plasmas **27**, 042703 (2020).

[18] C. S. Liu and M. N. Rosenbluth, Phys. Fluids **19**, 967 (1976).

[19] A. Simon, R. W. Short, E. A. Williams, and T. Dewandre, Phys. Fluids **26**, 3107 (1983).

[20] M. N. Rosenbluth, Phys. Rev. Lett. **29**, 565 (1972).

[21] M. N. Rosenbluth, R. B. White, and C. S. Liu, Phys. Rev. Lett. **31**, 1190 (1973).

[22] C. Z. Xiao, Y. G. Chen, J. F. Myatt, Q. Wang, Y. Chen, Z. J. Liu, C. Y. Zheng, and X. T. He, Phys. Rev. E **104**, 065203 (2021).

[23] J. F. Myatt, J. G. Shaw, R. K. Follett, D. H. Edgell, D. H. Froula, J. P. Palastro, and V. N. Goncharov, J. Comput. Phys. **399**, 108916 (2019).